Mechanical cues control mutant p53 stability through a mevalonate–RhoA axis

Eleonora Ingallina[1], Giovanni Sorrentino[1,9], Rebecca Bertolio[1,2], Kamil Lisek[1,10], Alessandro Zannini[1,2], Luca Azzolin[3], Luisa Ulloa Severino[2,4], Denis Scaini[2,4], Miguel Mano[5,6], Fiamma Mantovani[1,2], Antonio Rosato[7], Silvio Bicciato[8], Stefano Piccolo[3] and Giannino Del Sal[1,2*]

Tumour-associated p53 missense mutants act as driver oncogenes affecting cancer progression, metastatic potential and drug resistance (gain-of-function)[1]. Mutant p53 protein stabilization is a prerequisite for gain-of-function manifestation; however, it does not represent an intrinsic property of p53 mutants, but rather requires secondary events[2]. Moreover, mutant p53 protein levels are often heterogeneous even within the same tumour, raising questions on the mechanisms that control local mutant p53 accumulation in some tumour cells but not in their neighbours[2,3]. By investigating the cellular pathways that induce protection of mutant p53 from ubiquitin-mediated proteolysis, we found that HDAC6/Hsp90-dependent mutant p53 accumulation is sustained by RhoA geranylgeranylation downstream of the mevalonate pathway, as well as by RhoA- and actin-dependent transduction of mechanical inputs, such as the stiffness of the extracellular environment. Our results provide evidence for an unpredicted layer of mutant p53 regulation that relies on metabolic and mechanical cues.

Mutation of the *TP53* gene is the most frequent genetic lesion in human cancers[1]. Numerous studies have clearly established that missense p53 mutants are dependent on a transformed context for full activation of their malignant potential[4]. This includes oncogenic signalling, in response to which mutant p53 proteins are post-translationally modified[5], and tumour-specific mechanisms of protein hyper-stabilization[6] that oppose the inherent instability of p53 mutants observed in normal tissues[2]. Remarkably, mutant p53 accumulation has been reported to be often spatially heterogeneous in individual tumours[3,7], suggesting that its protein stability may be influenced by local environmental cues.

Aiming to identify cellular processes and biochemical pathways responsible for mutant p53 stabilization in cancer cells, we performed a high-content screening of FDA-approved drugs (Supplementary Fig. 1A)[8,9] in MDA-MB-231 breast cancer cells, in which we monitored the variations of mutant p53 levels after drug administration (Supplementary Table 1). On filtering the results by reproducibility, toxicity, dose dependence and manual inspection of images, the best hits associated with decreased levels of mutant p53 were the cardiac glycoside ouabain, the antipsychotics spiperone and thioridazine, the antiparasitic agent ivermectin, and two entire classes of drugs, namely adrenergic agonists (for example, salmeterol) and mevalonate pathway inhibitors (statins) (Fig. 1a–c, Supplementary Figs. 1B,C and 5B and Supplementary Table 2). None of the compounds identified by our screening was able to reduce p53 messenger RNA levels, thus suggesting a post-transcriptional mechanism of action (Supplementary Fig. 2A).

Confirming the reliability of our approach, adrenergic agonists (for example, isoprenaline) and ouabain have already been identified as p53-destabilizing agents[10,11]. Thus, for further analysis, we focused on statins, a class of drugs clinically used to lower cholesterol plasma levels in patients with cardiovascular disease. Statins act by inhibiting HMG-CoA reductase (HMGCR), which catalyses mevalonic acid (MVA) synthesis (the first rate-limiting step of the metabolic pathway leading to cholesterol biosynthesis, namely the mevalonate pathway)[12]. Cerivastatin and simvastatin behaved similarly in reducing mutant p53 levels (Fig. 1c and Supplementary Figs. 2B and 5B) and cerivastatin induced mutant p53 cytoplasmic localization (Supplementary Fig. 1D). The decrease in the level of mutant p53 following administration of cerivastatin was time-dependent and maximal after 48 h (Fig. 1d and Supplementary Fig. 5B). Cerivastatin also reduced the levels of exogenously expressed mutant p53 R280K in MDA-MB-231 cells (Fig. 1e and Supplementary Fig. 5B).

To assess whether the mevalonate pathway is a general regulator of mutant p53 levels, we analysed the effects of cerivastatin on a panel of human tumour cell lines harbouring different p53 mutants or wild-type p53. As shown in Fig. 1f, the treatment caused a substantial reduction of mutant p53 protein levels in all of the tested cell lines (Fig. 1f and Supplementary Fig. 2C), while wild-type p53 levels were unaffected (Fig. 1f and Supplementary Figs. 1I and 5B). Consistently, statin treatment reduced the proliferation of cells expressing missense mutant p53, with no effect on cells expressing wild-type p53 or null for p53 (Fig. 1g). Cerivastatin also induced mild cell death in MDA-MB-231 cells; however, inhibition of apoptosis by Z-VAD treatment did not prevent mutant p53 reduction, suggesting that mutant p53 levels were not altered as a consequence of cell death (Supplementary Fig. 1E). In line with this result, induction of apoptosis in MDA-MB-231 cells by doxorubicin or 5-FU treatment did not reduce mutant p53 levels (Supplementary Fig. 1F).

[1]Laboratorio Nazionale CIB, Area Science Park Padriciano, Trieste, Italy. [2]Dipartimento di Scienze della Vita, Università degli Studi di Trieste, Trieste, Italy. [3]Department of Molecular Medicine, School of Medicine, University of Padova, Padova, Italy. [4]NanoInnovation Lab at Elettra-Sincrotrone Trieste, Basovizza, Trieste, Italy. [5]Center for Neuroscience and Cell Biology, University of Coimbra, Coimbra, Portugal. [6]International Centre for Genetic Engineering and Biotechnology, Trieste, Italy. [7]Veneto Institute of Oncology IOV-IRCCS, Padova, Italy. [8]Department of Life Sciences, University of Modena and Reggio Emilia, Modena, Italy. Present addresses: [9]Laboratory of Metabolic Signaling, Institute of Bioengineering, Ecole Polytechnique Fédérale de Lausanne, Lausanne, Switzerland. [10]Max-Delbrück-Centrum for Molecular Medicine in Hemholtz Association, Berlin, Germany. Eleonora Ingallina and Giovanni Sorrentino contributed equally to this work. *e-mail: gdelsal@units.it

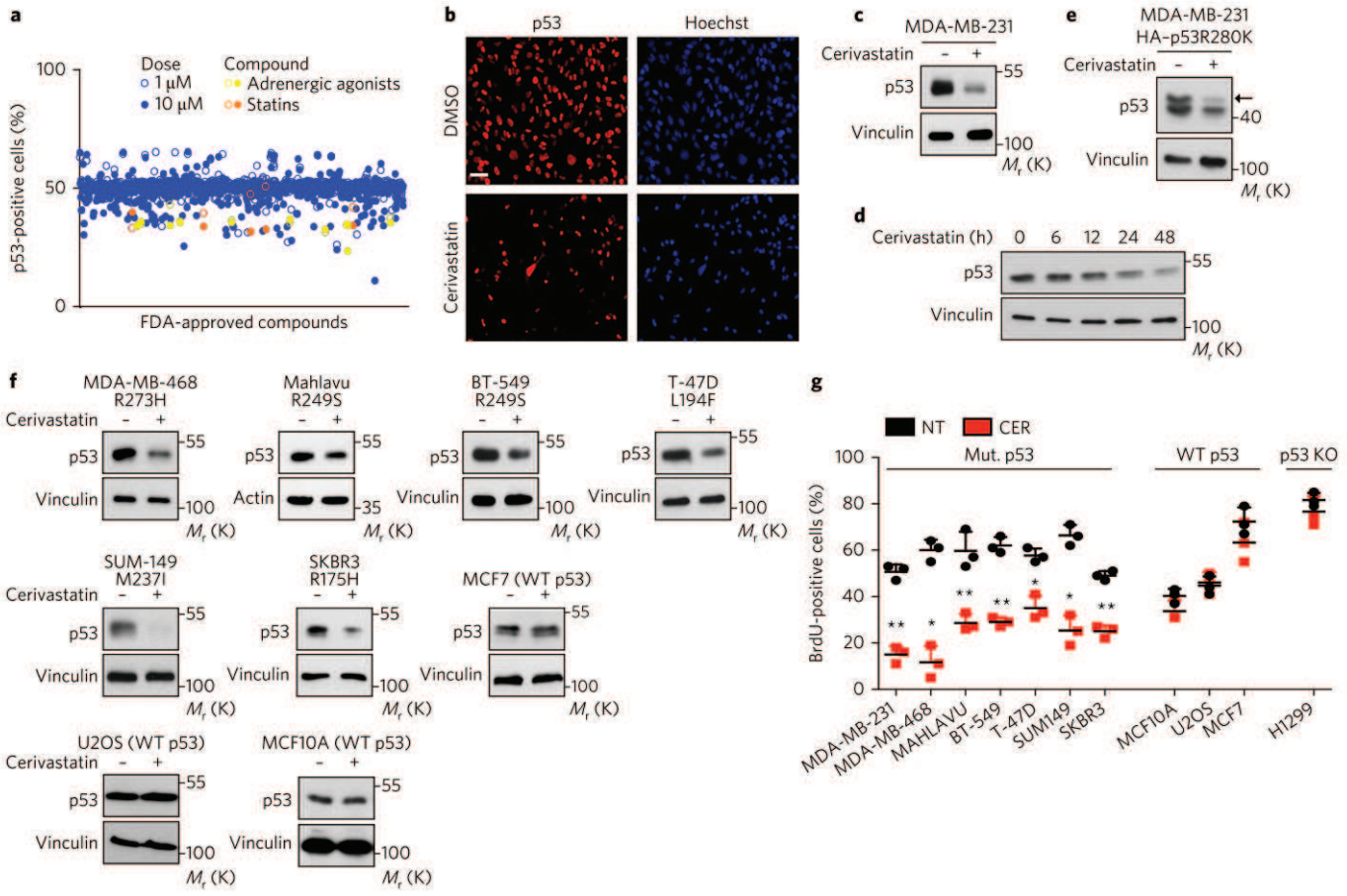

Fig. 1 | Statins reduce missense mutant p53 protein levels in cancer cells. a, The results of high-content screening. Mutant-p53-positive cells were detected by immunofluorescence and quantified through automated image analysis. **b**, Representative images of p53 immunofluorescence from the screening in **a**. MDA-MB-231 cells were treated with dimethylsulfoxide (DMSO) or cerivastatin (10 μM) for 24 h. Scale bar, 15 μm. **c**, MDA-MB-231 cells were treated with DMSO (–) or with cerivastatin (+; 10 μM) for 48 h. Representative western blots are shown. **d**, MDA-MB-231 cells were treated with cerivastatin 10 μM for the indicated time points. Representative western blots are shown. **e**, MDA-MB-231 cells expressing pcDNA3–HA–p53R280K vector were treated with DMSO (–) or treated with cerivastatin (+; 10 μM) for 48 h. Representative blots are shown. Arrow indicates overexpressed HA-tagged p53, lower band is endogenous p53. **f**, The indicated cell lines were treated with DMSO (–) or with cerivastatin (+; 10 μM) for 48 h. Representative blots are shown. **g**, Quantification of BrdU-positive cells. The indicated cell lines, expressing mutant (Mut.), wild type (WT), or knock-out (KO) p53, were untreated (NT) or treated with cerivastatin (CER; 0.1 μM) for 48 h. The error bars represent mean ± s.d. from $n = 3$ biologically independent experiments. $^{**}P < 0.01$, $^{*}P < 0.05$; P values (from left to right): 0.008; 0.016; 0.007; 0.008; 0.039; 0.017; 0.005; 0.266; 0.801; 0.221; 0.341. Two-tailed Student's t-test was used. All experiments were repeated three times, apart from that in **a**, which was performed twice. Source data for **g** are available in Supplementary Table 6. Unprocessed original scans of blots are shown in Supplementary Fig. 6.

In MDA-MB-231 cells, cerivastatin shortened the half-life of both endogenous and overexpressed mutant p53 in a proteasome-dependent manner (Fig. 2a and Supplementary Fig. 1G,H), and caused an increase of mutant p53 polyubiquitylated forms (Fig. 2b). On the basis of this and other evidence[2,13], we hypothesized that statins could reactivate the ubiquitin-dependent degradation of mutant p53 in cancer cells. Indeed, administration of the MDM2 inhibitor nutlin, as well as specific knockdown of MDM2 caused a significant rescue of mutant p53 stability in cerivastatin-treated MDA-MB-231 cells (Fig. 2a,c,d and Supplementary Figs. 1J and 5B), thus suggesting that statin treatment affects mutant p53 levels via the MDM2 ubiquitin ligase. Of note, neither treatment was able to completely rescue mutant p53 levels, implying the existence of additional mechanisms mediating mutant p53 inhibition by statins.

In cancer cells, mutant p53 proteins are engaged in stable complexes with the Hsp90 chaperone, which is often upregulated during transformation[14]. This interaction results in a marked reduction of mutant p53 ubiquitylation by the E3 ligase MDM2 (Fig. 2e)[15,16]. As shown in Fig. 2f, cerivastatin caused the dissociation of Hsp90 from mutant p53, while its binding to MDM2 was unaffected (Supplementary Fig. 5B). These data suggest that inhibition of the mevalonate pathway in cancer cells restores the inherent instability of mutant p53 by functionally disrupting the molecular mechanism protecting mutant p53 from inhibition by MDM2.

It has been shown that HDAC6-mediated Hsp90 deacetylation fosters mutant p53 stabilization[17,18]. Of note, statins have been found to inhibit HDAC enzymatic activity in tumour cells[19,20]. We thus hypothesized that HMGCR inhibition could reduce HDAC6 activity, leading to Hsp90 acetylation (inactivation) and mutant p53 destabilization. As shown in Supplementary Fig. 2D, cerivastatin treatment indeed inhibited HDAC6, leading to increased tubulin acetylation. Of note, cerivastatin treatment induced an increase of Hsp90 acetylation, which was comparable to that induced by sulforaphane (a HDAC6 inhibitor[17,21]) (Supplementary Fig. 2E). These results suggest that HMGCR inhibition reduces Hsp90 activity as a consequence of HDAC6 inhibition.

All enzymes belonging to the mevalonate pathway are under direct transcriptional control of sterol regulatory element-binding

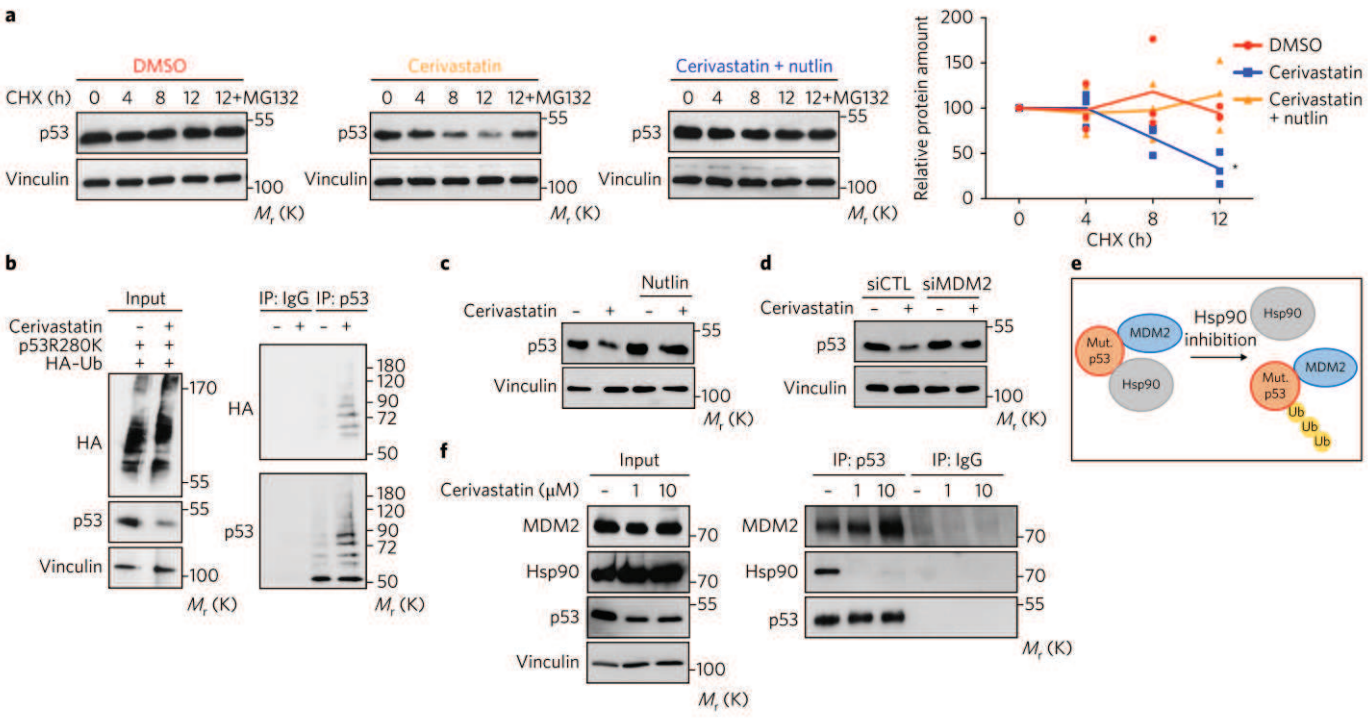

Fig. 2 | Statins unleash MDM2-mediated degradation of mutant p53 by disrupting its interaction with Hsp90. a, Evaluation of mutant p53 half-life in MDA-MB-231 cells. Cells were pre-treated with DMSO or cerivastatin (1 μM), alone or with nutlin (10 μM), and after 24 h cells were treated with cycloheximide (CHX; 50 μM) for the indicated times. MG132 (50 μM) was added after 12 h to inhibit the proteasome. Representative western blots with the indicated antibodies are shown. The graph indicates normalized quantification of mutant p53 protein amounts. Each replicate from $n=3$ biologically independent experiments is shown. *$P=0.012$. Two-tailed Student's *t*-test. **b**, Left: MDA-MB-231 cells were transfected with constructs expressing HA-ubiquitin and pcDNA3-p53R280K and then treated with cerivastatin (1 μM) for 48 h. Right: mutant p53 was immunoprecipitated from lysates and an anti-HA blot was performed to detect ubiquitylated forms of mutant p53. **c**, MDA-MB-231 cells were treated with Nutlin-3 (10 μM) for 12 h and then cerivastatin (10 μM) was added to the medium for an additional 48 h. Representative blots are shown. **d**, MDA-MB-231 cells were treated with cerivastatin (10 μM) for 48 h after transfection with the indicated siRNA for 24 h. Representative blots are shown. **e**, Schematic representation of the mechanism of mutant p53 stabilization by Hsp90 in cancer cells. **f**, Mutant p53 was immunoprecipitated from lysates of MDA-MB-231 cells, untreated (-) or treated with cerivastatin (1 or 10 μM) for 24 h (left) . Co-immunoprecipitated Hsp90 and MDM2 were detected by western blot (right). All experiments were repeated three independent times with similar results. Source data for **a** are available in Supplementary Table 6. Unprocessed original scans of blots are shown in Supplementary Fig. 6.

protein (SREBP) transcription factors (Fig. 3a)[22]. Knockdown of either SREBP1 or SREBP2 in MDA-MB-231 cells coincided with a significant decrease of mutant p53 protein levels (Fig. 3b and Supplementary Fig. 5B). Conversely, activation of endogenous SREBP1/2 by culturing cells in lipoprotein-depleted serum increased mutant p53 protein levels, and this effect was nullified by inhibiting the mevalonate pathway with statins (Fig. 3c and Supplementary Fig. 5B). Remarkably, mutant p53 protein levels were rescued in cerivastatin-treated MDA-MB-231 cells by addition of MVA, consistent with mutant p53 levels being dependent on intracellular mevalonate levels (Fig. 3d and Supplementary Fig. 5B). These results demonstrate that activation of the SREBP–mevalonate pathway promotes the accumulation of mutant p53 protein in cancer cells.

In addition to being responsible for de novo biosynthesis of cholesterol, the mevalonate pathway is essential for the production of other key metabolites, such as farnesyl pyrophosphate and geranylgeranyl pyrophosphate (Fig. 3a)[23]. Interestingly, only the geranylgeranyl transferase 1 (GGTase1) inhibitor GGTI-298 and the farnesyl di-phosphate synthase inhibitor zoledronic acid (ZA) were able to phenocopy the effect of statins on mutant p53, whereas the inhibition of squalene synthase by YM-53601 and farnesyl transferase by FTI-277 were ineffective (Fig. 3e,f and Supplementary Fig. 5B). GGTI-298 treatment induced MDM2-dependent mutant p53 ubiquitylation (Supplementary Fig. 2F), due to inhibition of HDAC6, consequent increase of Hsp90 acetylation and dissociation of mutant p53 (Fig. 3i and Supplementary Figs. 2D,E and 5B). The effects of GGTI-298 were partially rescued by either proteasome or MDM2 inhibition (Supplementary Fig. 2G,H). Geranylgeranyl pyrophosphate (GGPP) addition to statin-treated cells, instead, rescued both mutant p53 levels (Fig. 3g and Supplementary Fig. 5B) and activation (as measured by the expression of the 'ten genes' signature[5], Supplementary Fig. 4A) as well as cell proliferation (Fig. 3h and Supplementary Fig. 4B). These data indicate that protein geranylgeranylation is required for mutant p53 accumulation in cancer cells.

The main biological role of geranylgeranylation is anchoring proteins to cellular membranes[24]. Rho-GTPases represent major GGTase1 targets and statins have been found to inhibit the enzymatic activity of RhoA[8]. Interestingly, RhoA has recently been identified as a key mediator of the anti-tumour activity of statins, and a crucial target of mutant p53 in controlling cellular metabolism[8,12,25,26]. Therefore, we asked whether RhoA might control mutant p53 levels downstream of MVA. Strikingly, inhibition of RhoA, by means of either short interfering RNA (siRNA) or treatment with its specific inhibitor C3 toxin, was able to reduce mutant p53 protein levels in different cancer cell lines (Fig. 4a,b and Supplementary Figs. 2I,J and 5B). As expected, treatment of MDA-MB-231 cells with C3 shortened mutant p53 half-life (Supplementary Fig. 2K). Conversely, overexpression of a constitutively active form of RhoA

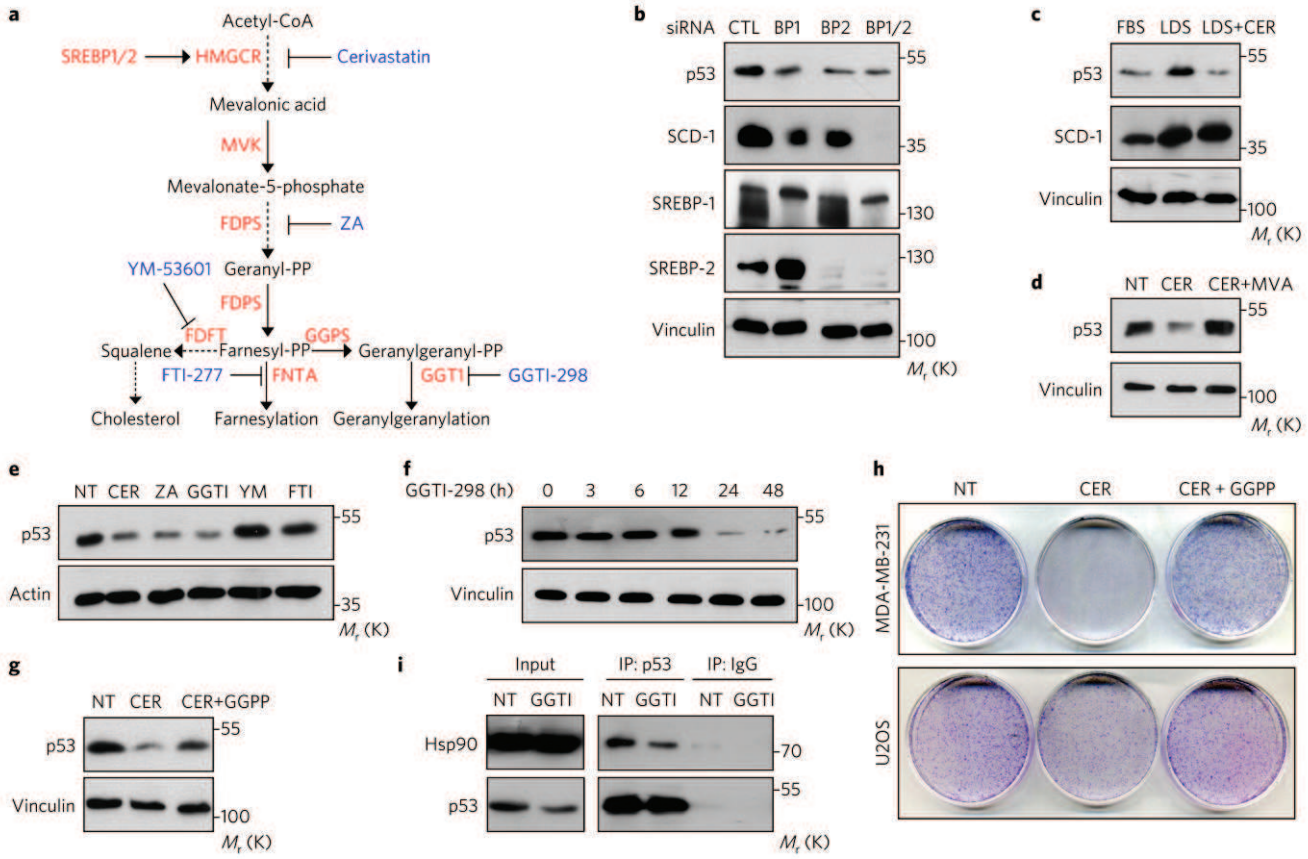

Fig. 3 | The SREBP–mevalonate pathway controls mutant p53 levels via GGPP. a, Schematic overview of the mevalonate pathway. Enzymes are shown in red and inhibitors are shown in blue. **b**, MDA-MB-231 cells transfected with siRNAs targeting either SREBP1 (BP1) or SREBP2 (BP2) or SREBP1/2 together (BP1/2) for 48 h. Representative western blots with the indicated antibodies are shown. SCD-1, a SREBP1/2 target involved in lipid metabolism, was used as a positive control. CTL, control vector. **c**, MDA-MB-231 cells were grown in medium supplemented with 10% FBS or 2% lipoprotein-depleted serum (LDS) with or without cerivastatin (CER; 10 μM) for 48 h. Representative blots are shown. **d**, MDA-MB-231 cells were treated with cerivastatin (CER; 10 μM) alone or with mevalonic acid (MVA; 0.5 mM) for 48 h. Representative blots are shown. **e**, MDA-MB-231 cells were treated with different inhibitors: cerivastatin (CER; 10 μM), zoledronic acid (ZA; 50 μM), geranylgeranyl transferase I inhibitor (GGTI-298; 10 μM), squalene synthase inhibitor (YM-53601; 20 μM), farnesyl transferase inhibitor (FTI-277; 20 μM), for 48 h. Representative blots are shown. **f**, MDA-MB-231 cells were treated with GGTI-298 (10 μM) for the indicated times. Representative blots are shown. **g**, MDA-MB-231 cells were treated with cerivastatin (CER; 10 μM) either alone or in combination with geranylgeranyl pyrophosphate (GGPP; 20 μM) for 48 h. Representative blots are shown. **h**, Colony-formation assay. The indicated cell lines were treated with cerivastatin (CER; 0.1 μM) either alone or in combination with geranylgeranyl pyrophosphate (GGPP; 20 μM) for six days. **i**, Mutant p53 was immunoprecipitated from lysates of MDA-MB-231 cells either untreated (NT) or treated with GGTI-298 (10 μM) for 24 h (left). Co-immunoprecipitated Hsp90 was detected by western blot (right). All experiments were repeated three independent times with similar results. Unprocessed original scans of blots are shown in Supplementary Fig. 6.

(RhoA-G14V) in MDA-MB-231 cells induced mutant p53 accumulation and activation (Fig. 4c and Supplementary Figs. 2L, 4C and 5B) that were completely prevented by treatment with GGTase1 inhibitor (Fig. 4c and Supplementary Fig. 5B). Importantly, in cells expressing a statin-sensitive but GGTI-insensitive GFP–RhoA mutant (RhoA-G14V-F)[8,27], GGTase1 inhibition was less efficient in reducing mutant p53 levels and cell proliferation (Fig. 4d and Supplementary Figs. 2M,N and 5B), thus proving that RhoA prenylation is required for mutant p53 accumulation. Finally, knockdown of RhoA expression reduced the binding of Hsp90 to mutant p53 (Fig. 4f and Supplementary Fig. 5B). Together, these results implicate the activation of RhoA in the regulation of mutant p53 protein levels.

RhoA is a master regulator of actin cytoskeleton rearrangements and its activity is fundamental for transducing mechanical inputs generated by the extracellular/intracellular environment[28]. Thus, we asked whether acto-myosin dynamics control mutant p53 levels downstream of mevalonate–RhoA signalling. First, we analysed the impact of the mevalonate pathway on actomyosin dynamics by treating cells with cerivastatin, and monitoring phalloidin and pMLC2(Ser19) staining, as readouts of F-actin polymerization and of RhoA-dependent contractile myosin, respectively. Strikingly, inhibition of the mevalonate pathway by statin or ZA caused a dramatic reduction in both F-actin polymerization and MLC2 phosphorylation, as also observed following latrunculin A treatment, suggesting that the mevalonate pathway is functionally required for RhoA-dependent mechanotransduction in vitro (Fig. 5a and Supplementary Fig. 3A,B). A direct demonstration of actin cytoskeleton de-structuring has been provided by the significant reduction in cell stiffness observed in ZA- and statin-treated cells ($P<0.001$), and measured by means of atomic force microscopy (AFM) (Fig. 5b). Similar effects have been observed in blebbistatin- or Rho-kinase (ROCK)-inhibitor treated cells (Fig. 5b). Interestingly, geranylgeranyl pyrophosphate was able to reverse statin effects, increasing cellular stiffness to levels comparable to those observed in untreated cells (Fig. 5b). To test whether disruption of actin

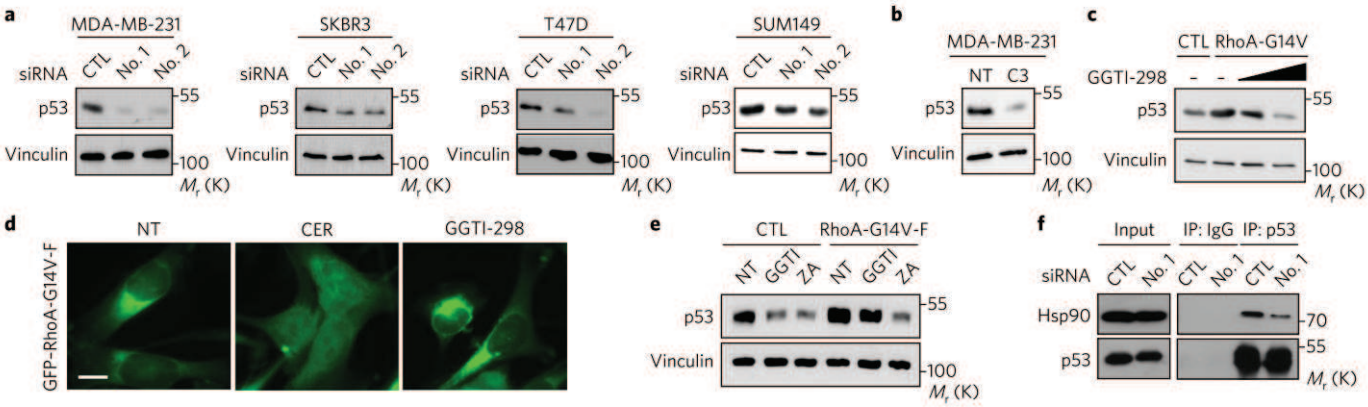

Fig. 4 | RhoA geranylgeranylation controls mutant p53 levels downstream of the mevalonate pathway. a, The indicated cell lines were transfected with two independent siRNAs targeting RhoA for 72 h. Representative blots are shown. **b**, MDA-MB-231 cells were treated with C3 toxin (100 ng ml^{-1}) for 48 h. Representative blots are shown. **c**, MDA-MB-231 cells stably expressing control vector (CTL) or the active form of RhoA (RhoA-G14V) were treated with increasing amount of GGTI-298 (0; 10 μM; 20 μM) for 48 h. Representative blots are shown. **d**, Fluorescence microscopy analysis of MDA-MB-231 cells stably expressing the construct coding for a mutant RhoA-G14V bearing a farnesylation consensus sequence (GFP–RhoA-G14V-F) either left untreated (NT) or treated with cerivastatin (CER; 1 μM) or with GGTI-298 (10 μM) for 48 h. Scale bar, 15 μm. **e**, MDA-MB-231 cells stably expressing control vector (CTL) or GFP–RhoA-G14V-F were left untreated (NT) or treated with GGTI-298 (10 μM) or zoledronic acid (ZA; 50 μM) for 48 h. Representative blots are shown. **f**, Mutant p53 was immunoprecipitated from lysates of MDA-MB-231 cells transfected with control (CTL) or two independent RhoA siRNAs (siRNA no. 1) for 72 h (left). Co-immunoprecipitated Hsp90 was detected by western blot (right). All experiments were repeated three independent times with similar results. Unprocessed original scans of blots are shown in Supplementary Fig. 6.

cytoskeleton affects mutant p53 levels, we administrated latrunculin A to MDA-MB-231 cells and stained cells for F-actin and p53. As shown in Fig. 5c, latrunculin A elicited attenuation of F-actin stress fibres and concomitant reduction of mutant p53 levels (Fig. 5c and Supplementary Fig. 3E). Similarly, actin contractility inhibition or Rho-Kinase inhibition reduced mutant p53 levels (Fig. 5b and Supplementary Fig. 3C,D). Of note, in statin-treated cells, the effect of mevalonate addition on mutant p53 levels was nullified by latrunculin A (Supplementary Fig. 3F). These results suggest that RhoA-dependent acto-myosin dynamics affect mutant p53 levels in tumour cells.

We then evaluated the role of the mevalonate pathway in tumour mechanosignalling and the effects of this on mutant p53 accumulation in vivo. To this end, we used archival tumour tissues from nude mice orthotopically injected with MDA-MB-231 cells and treated with ZA. In these mice, ZA caused a significant reduction of tumour growth[8]. Tumour tissues were then analysed for markers of mechanosignalling and for mutant p53 levels. Of note, tumour samples from mice receiving ZA showed a robust reduction of mechanosignalling, as indicated by decreased phosphorylation of focal adhesion kinase (pFAK residue Tyr397) and of myosin light chain 2 (pMLC2 residue Ser19) (Fig. 5d). Accordingly, ZA treatment significantly decreased mutant p53 levels (Fig. 5d). Interestingly, AFM analysis of tumour tissues showed that ZA treatment also reduced the stiffness of the cancer cells and of the extracellular matrix within the tumour (Supplementary Fig. 3O).

Aberrant tissue tensional homeostasis is a feature of several epithelial cancers[29]. In this context, RhoA becomes activated by tissue rigidity and is part of an integrated mechanoregulatory circuit linking extracellular matrix stiffness to cytoskeletal tension (Supplementary Fig. 3G,H)[29]. On the basis of these premises, we postulated that matrix stiffness might act as an environmental input promoting mutant p53 stabilization through mevalonate–RhoA-mediated mechanosignalling. To verify this hypothesis, we employed a pre-neoplastic experimental system, mammary epithelial cells (MECs) isolated from 8-week-old p53$^{R172H/R172H}$ knock-in mice. These cells were grown either on a soft fibronectin-coated hydrogel matching the compliance of normal mammary tissue (Young's modulus: 0.5 kPa)[29,30], or on a stiff fibronectin-coated hydrogel (Young's modulus: 50 kPa) (Fig. 5e and Supplementary Fig. 5B). As expected, mutant p53 levels were almost undetectable in MECs plated on soft matrix, confirming that the protein is intrinsically unstable in non-transformed tissues (Fig. 5e). Strikingly, however, mutant p53 accumulated at high levels when MECs were grown on a hyperstiff matrix, and inhibition of the mevalonate pathway by cerivastatin treatment prevented its accumulation (Fig. 5e). Cancer cells grown on soft fibronectin-coated hydrogels also showed significantly lower mutant p53 protein levels and activation (measured by the 'ten genes' signature[5]) (Fig. 5f and Supplementary Fig. 3H,N) as well as reduced levels of the enzymes involved in protein geranylgeranylation (namely Ggps1 and GGTase-1) and RhoA activation (Supplementary Fig. 3G,I). Of note, inhibition of actin polymerization by latrunculin A and treatment with cerivastatin both reduced mutant p53 levels and activation with similar efficiency (Fig. 5f and Supplementary Fig. 5B). Overexpression of activated RhoA (RhoA-G14V) in cells grown on soft matrix efficiently promoted stabilization of mutant p53 to levels observed in cells grown on plastic (Fig. 5g and Supplementary Fig. 5B). Notably, in cells grown on soft hydrogels, Hsp90 is acetylated due to HDAC6 inhibition, and consequently is less efficient in binding mutant p53 (Fig. 5h and Supplementary Figs. 2D,E and 5B). Finally, while growing cells on stiff matrix induced mutant p53 accumulation, the concomitant inhibition of HDAC6 prevented this effect (Fig. 5i and Supplementary Figs. 3J,K and 5B), thus demonstrating the functional requirement of HDAC6 for mutant p53 stabilization downstream of RhoA/mechanical cues. These results demonstrate that mutant p53 proteins are not intrinsically stable in tumour cells, rather their accumulation is strongly influenced by the mevalonate–RhoA axis and by mechanical cues such as the stiffness of the extracellular environment.

We then decided to verify whether increased mechanosignalling correlates with mutant p53 activation in human tumours. To this end, we performed and validated gene expression analysis on MDA-MB-231 cells grown on either a soft or stiff surface and generated a 'stiffness' signature, composed of genes induced in stiff as compared with soft matrix (Supplementary Fig. 4D and Supplementary

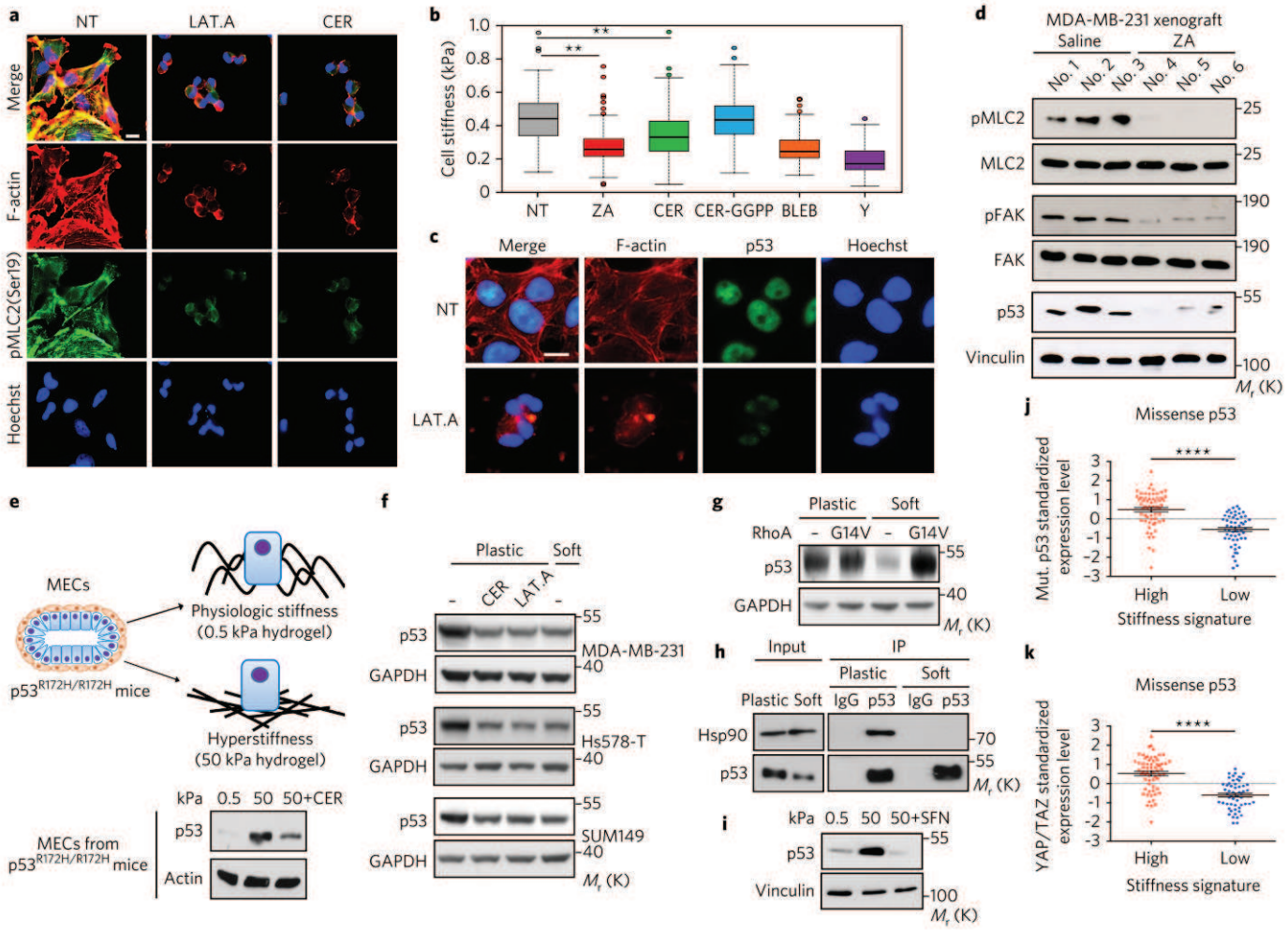

Fig. 5 | Mechanical cues control mutant p53 levels and activity via RhoA/actin cytoskeleton. a, MDA-MB-231 cells were treated with latrunculin A (LAT.A; 0.5 μM) or cerivastatin (CER; 10 μM) for 48 h. Scale bar, 15 μm. **b**, Cell stiffness 48 h after treatment with the indicated compounds. BLEB, blebbistatin; Y, Y-27632 dihydrochloride. Data for NT come from $n=291$ cells (pooled across five independent experiments), data for ZA, CER and CER-GGPP come from $n=171$, $n=156$ and $n=163$ cells, respectively (pooled across three independent experiments each), and data for BLEB and Y come from $n=114$ and $n=110$ cells, respectively (pooled across two independent experiments each). Box plots range from 25th to 75th percentiles, and the bold lines inside the box represent the median. *P* values are obtained by a two-sample Kolmogorov–Smirnov test based on probability distribution. $^{**}P<0.01$. **c**, MDA-MB-231 cells were treated with latrunculin A (LAT.A; 0.5 μM) for 48 h. Scale bar, 15 μm. **d**, Lysates of MDA-MB-231-derived xenograft tumours from saline- or zoledronic acid (ZA)-treated mice. **e**, Upper: schematic overview of the experiment. Lower: mammary epithelial cells (MECs) were plated on soft (0.5) or stiff (50) fibronectin-coated hydrogels for three days with or without cerivastatin (CER; 10 μM). **f**, The indicated cell lines were either grown on plastic, or plated on soft fibronectin-coated hydrogels for three days. Cells grown on plastic were also treated with latrunculin A (LAT.A; 0.5 μM) or cerivastatin (10 μM) for the last 48 h. **g**, SUM149 cells stably expressing control vector – or the active form of RhoA (G14V) were plated on plastic or on fibronectin-coated soft hydrogels for three days. **h**, Mutant p53 was immunoprecipitated from lysates of MDA-MB-231 cells grown on plastic, or plated on soft hydrogels for three days. **i**, MDA-MB-231 cells were plated on soft or stiff hydrogels for three days with or without sulforaphane (SFN; 20 μM). **j**, Average gene expression values of 'mutant p53 signature' genes in missense mutant p53 breast cancer samples[31], classified according to the 'stiffness' signature (determined by MDA 231 array). **k**, Average gene expression values of 'YAP/TAZ signature' genes in missense mutant p53 breast cancer samples[32], classified according to the 'stiffness' signature (as in **j**). In **k** and **j**, data are shown as individual samples ($n=117$ independent breast cancer patients, dots, obtained from the Molecular Taxonomy of Breast Cancer International Consortium, METABRIC) and the mean ± s.e.m. (standard error of the mean; back lines). $^{****}P<0.0001$ in a two-tailed unpaired *t*-test. The experiments in **a**,**e**–**i** were repeated three independent times with similar results. The experiment in **d** was performed once. Unprocessed original scans of blots are shown in Supplementary Fig. 6.

Table 5). Next, we interrogated a data set of 117 missense mutant p53 human breast cancers and classified tumours as having high or low expression of this 'stiffness' signature. When we monitored the activation of mutant p53 in these tumours, by analysing expression of a published 'mutant p53 signature'[31], we found that tumours classified as 'highly stiff' were also characterized by strong activation of mutant p53 (Fig. 5j). As a positive control, the YAP/TAZ signature[32] was also upregulated in the same specimens[32–34], indicating a parallel between activation of a widely validated mechanosensitive cascade and of mutant p53 in primary human tumours (Fig. 5k and Supplementary Fig. 5A). These observations confirm that mutant p53 is more active in cells with activated mechanosignalling. Of note, YAP/TAZ were not involved in mutant p53 stabilization, as YAP or YAP/TAZ knockdown had no effects on mutant p53 levels in stiff matrix or in cells overexpressing the active form of RhoA (Supplementary Fig. 3L,M).

In cancer cells, the mevalonate pathway can be activated by a direct mutant p53–SREBP interaction, which sustains SREBP transcriptional activity[35]. Combined with our finding that SREBP activation affects mutant p53 levels, this evidence supports the concept that in cancer cells mutant p53 can give rise to a positive feedback loop in which, by forcing mevalonate pathway activation and GGPP biosynthesis, mutant p53 can sustain its own stabilization. RhoA geranylgeranylation turns out to be an essential process in these events. This interplay could possibly require other proteins, such as HDAC6[17,36,37]. The Rho pathway may work in concert with other, possibly redundant or tumour-specific mechanisms to stabilize mutant p53. For example, activation of the Hsp40/DNAJ chaperone by the mevalonate pathway has recently been found to control mutant p53 stability[38] through the ubiquitin ligase chromatin immunoprecipitation. Although the involvement of cell mechanics was not investigated in that study, our work nonetheless defines a different pathway, involving Hsp90 and MDM2.

More importantly, we demonstrate that pharmacologic inhibition of the mevalonate–RhoA axis (for example, by statins, ZA or GGTI) can interfere with the transduction of mechanical inputs in vitro and in vivo and thereby prevent the stabilization of mutant p53 and of other oncogenes such as YAP/TAZ[8], ultimately restraining diverse malignant cancer phenotypes.

Mutant p53 accumulation is often spatially heterogeneous within primary tumours, with mutant-p53-overexpressing tumour foci associated with fibrous stroma[3]. Our work shows that the extracellular microenvironment controls mutant p53 stabilization and activation. On this basis, we speculate that the heterogeneity of mutant p53 expression observed within individual tumours might be explained by different mechanical niches existing within the diseased tissues[30]. The presence of fibrotic 'stiff' lesions, along with influencing treatment efficacy[39], is associated with poor prognosis[40], enhanced growth and survival signalling, and with invasive and pro-metastatic features[29]. Our results imply that conditions that increase ECM stiffening (fibrosis) and cell contractility in mutant p53 tumours could induce stabilization of mutant p53 and activation of its oncogenic properties, ultimately facilitating malignant progression.

Accepted 15 November 2017

References

1. Mantovani, F., Walerych, D. & Del Sal, G. Targeting mutant p53 in cancer: a long road to precision therapy. *FEBS J.* **284**, 837–850 (2016).
2. Terzian, T. et al. The inherent instability of mutant p53 is alleviated by *Mdm2* or *p16^{INK4a}* loss. *Genes Dev.* **22**, 1337–1344 (2008).
3. Koga, T. et al. Heterogeneous distribution of P53 immunoreactivity in human lung adenocarcinoma correlates with MDM2 protein expression, rather than with P53 gene mutation. *Int. J. Cancer* **95**, 232–239 (2001).
4. Freed-Pastor, W. A. & Prives, C. Mutant p53: one name, many proteins. *Genes Dev.* **26**, 1268–1286 (2012).
5. Girardini, J. E. et al. A Pin1/mutant p53 axis promotes aggressiveness in breast cancer. *Cancer Cell* **20**, 79–91 (2011).
6. Ashcroft, M. & Vousden, K. H. Regulation of p53 stability. *Oncogene* **18**, 7637–7643 (1999).
7. Bouchalova, P. et al. Mutant p53 accumulation in human breast cancer is not an intrinsic property or dependent on structural or functional disruption but is regulated by exogenous stress and receptor status. *J. Pathol.* **233**, 238–246 (2014).
8. Sorrentino, G. et al. Metabolic control of YAP and TAZ by the mevalonate pathway. *Nat. Cell Biol.* **16**, 357–366 (2014).
9. Sorrentino, G. et al. Glucocorticoid receptor signalling activates YAP in breast cancer. *Nat. Commun.* **8**, 14073 (2017).
10. Wang, Z. et al. Cardiac glycosides inhibit p53 synthesis by a mechanism relieved by Src or MAPK inhibition. *Cancer Res.* **69**, 6556–6564 (2009).
11. Hara, M. R. et al. A stress response pathway regulates DNA damage through β_2-adrenoreceptors and β-arrestin-1. *Nature* **477**, 349–353 (2011).
12. Mullen, P. J., Yu, R., Longo, J., Archer, M. C. & Penn, L. Z. The interplay between cell signalling and the mevalonate pathway in cancer. *Nat. Rev. Cancer* **16**, 718–731 (2016).
13. Lukashchuk, N. & Vousden, K. H. Ubiquitination and degradation of mutant p53. *Mol. Cell. Biol.* **27**, 8284–8295 (2007).
14. Malkin, D. Li-fraumeni syndrome. *Genes Cancer* **2**, 475–84 (2011).
15. Esser, C., Scheffner, M. & Höhfeld, J. The chaperone-associated ubiquitin ligase CHIP is able to target p53 for proteasomal degradation. *J. Biol. Chem.* **280**, 27443–27448 (2005).
16. Nagata, Y. et al. The stabilization mechanism of mutant-type p53 by impaired ubiquitination: the loss of wild-type p53 function and the hsp90 association. *Oncogene* **18**, 6037–6049 (1999).
17. Li, D., Marchenko, N. D. & Moll, U. M. SAHA shows preferential cytotoxicity in mutant p53 cancer cells by destabilizing mutant p53 through inhibition of the HDAC6-Hsp90 chaperone axis. *Cell Death Differ.* **18**, 1904–1913 (2011).
18. Kovacs, J. J. et al. HDAC6 regulates Hsp90 acetylation and chaperone-dependent activation of glucocorticoid receptor. *Mol. Cell* **18**, 601–607 (2005).
19. Lin, Y. C. et al. Statins increase p21 through inhibition of histone deacetylase activity and release of promoter-associated HDAC1/2. *Cancer Res.* **68**, 2375–2383 (2008).
20. Feig, J. E. et al. Statins promote the regression of atherosclerosis via activation of the CCR7-dependent emigration pathway in macrophages. *PLoS ONE* **6**, e28534 (2011).
21. Clarke, J. D., Hsu, A., Yu, Z., Dashwood, R. H. & Ho, E. Differential effects of sulforaphane on histone deacetylases, cell cycle arrest and apoptosis in normal prostate cells versus hyperplastic and cancerous prostate cells. *Mol. Nutr. Food Res.* **55**, 999–1009 (2011).
22. Brown, M. S. & Goldstein, J. L. The SREBP pathway: regulation of cholesterol metabolism by proteolysis of a membrane-bound transcription factor. *Cell* **89**, 331–340 (1997).
23. Repko, E. M. & Maltese, W. A. Post-transitional isoprenylation of cellular proteins is altered in response to mevalonate availability. *J. Biol. Chem.* **264**, 9945–9952 (1989).
24. Zhang, F. L. & Casey, P. J. Protein prenylation: molecular mechanisms and functional consequences. *Annu. Rev. Biochem.* **65**, 241–269 (1996).
25. Wang, Z. et al. Interplay of mevalonate and Hippo pathways regulates RHAMM transcription via YAP to modulate breast cancer cell motility. *Proc. Natl Acad. Sci. USA* **111**, E89–E98 (2014).
26. Zhang, C. et al. Tumour-associated mutant p53 drives the Warburg effect. *Nat. Commun.* **4**, 2935 (2013).
27. Mi, W. et al. Geranylgeranylation signals to the Hippo pathway for breast cancer cell proliferation and migration. *Oncogene* **34**, 3095–3106 (2014).
28. Ingber, D. E. Cellular mechanotransduction: putting all the pieces together again. *FASEB J.* **20**, 811–822 (2006).
29. Butcher, D. T., Alliston, T. & Weaver, V. M. A tense situation: forcing tumour progression. *Nat. Rev. Cancer* **9**, 108–22 (2009).
30. Janmey, P. A. & Miller, R. T. Mechanisms of mechanical signaling in development and disease. *J. Cell Sci.* **124**, 9–18 (2011).
31. Miller, L. D. et al. An expression signature for p53 status in human breast cancer predicts mutation status, transcriptional effects, and patient survival. *Proc. Natl Acad. Sci. USA* **102**, 13550–513555 (2005).
32. Zanconato, F. et al. Genome-wide association between YAP/TAZ/TEAD and AP-1 at enhancers drives oncogenic growth. *Nat. Cell Biol.* **17**, 1218–1227 (2015).
33. Aragona, M. et al. A mechanical checkpoint controls multicellular growth through YAP/TAZ regulation by actin-processing factors. *Cell* **154**, 1047–1059 (2013).
34. Zanconato, F., Cordenonsi, M. & Piccolo, S. YAP/TAZ at the roots of cancer. *Cancer Cell* **29**, 783–803 (2016).
35. Freed-Pastor, W. A. et al. Mutant p53 disrupts mammary tissue architecture via the mevalonate pathway. *Cell* **148**, 244–258 (2012).
36. Destaing, O. et al. A novel Rho-mDia2-HDAC6 pathway controls podosome patterning through microtubule acetylation in osteoclasts. *J. Cell Sci.* **118**, 2901–2911 (2005).
37. Boyault, C., Sadoul, K., Pabion, M. & Khochbin, S. HDAC6, at the crossroads between cytoskeleton and cell signaling by acetylation and ubiquitination. *Oncogene* **26**, 5468–5476 (2007).
38. Parrales, A. et al. DNAJA1 controls the fate of misfolded mutant p53 through the mevalonate pathway. *Nat. Cell Biol.* **18**, 1233–1243 (2016).
39. Netti, P. A., Berk, D. A., Swartz, M. A., Grodzinsky, A. J. & Jain, R. K. Role of extracellular matrix assembly in interstitial transport in solid tumours. *Cancer Res.* **60**, 2497–2503 (2000).
40. Colpaert, C. G. et al. The presence of a fibrotic focus in invasive breast carcinoma correlates with the expression of carbonic anhydrase IX and is a marker of hypoxia and poor prognosis. *Breast Cancer Res. Treat.* **81**, 137–147 (2003).

Acknowledgements

We thank A. Testa for discussions and proofreading the manuscript. We acknowledge G. Pastore for technical support. We thank S. Giulitti for preparation of hydrogels. We acknowledge support by the Italian Health Ministry (RF-2011-02346976 to G.D.S. and GR-2011-02348707 to D.S.), the Italian University and Research Ministry (PRIN-2015-8KZKE3), the Cariplo Foundation (grant no. 2014-0812) and Beneficentia-Stiftung to G.D.S. This work was supported by grants from the Associazione Italiana per la Ricerca sul Cancro (AIRC) and AIRC Special Program Molecular Clinical Oncology '5 per mille' (grant no. 10016) to G.D.S., S.B., A.R. and S.P., and AIRC IG (grant no. 17659) to G.D.S. This project has received funding from the European Research Council (ERC) under the European Union's Horizon 2020 research and innovation programme (grant agreement no. 670126-DENOVOSTEM) and an AIRC PI-Grant and by Epigenetics Flagship project CNR-Miur grants to S.P. M.M. is supported by the FIRB RBAP11Z4Z9 project from the Italian Ministry of Education and the FCT Investigator Programme IF/00694/2013 from the Portuguese Foundation for Science and Technology (FCT), Portugal. R.B. is a fellow of the Fondazione Italiana per la Ricerca sul Cancro (FIRC).

Author contributions

E.I., G.S., K.L., R.B., A.Z. and L.A. performed the experiments. A.R. performed mouse experiments. M.M. performed the high-content screening. S.B. performed bioinformatic analysis. D.S. and L.U.S. performed AFM experiments. G.S., E.I. and G.D.S. designed experiments. G.S., F.M., S.P. and G.D.S. wrote the manuscript.

Competing interests

The authors declare no competing financial interests.

Correspondence and requests for materials should be addressed to G.D.S.

Methods

Cell lines. MDA-MB-231 (p53 R280K), MDA-MB-468 (p53 R273H), SUM149 (p53 M237I), BT-549 (p53 R249S), SK-BR-3 (p53 R175H), T47D (p53 L194F) and Hs-578-T (p53 V157F) are human breast cancer cell lines. Mahlavu (p53 R249S) are human hepatocellular carcinoma cells. U118MG (p53 R213Q) are human glioblastoma cells. U2OS, an osteosarcoma cell line, and MCF-7, a human adenocarcinoma cell line, express wild-type p53, while H1299, a non-small cell lung cancer cell line, are p53 null.

MDA-MB-231, MDA-MB-468, BT-549, SKBR-3, U2OS, U118MG and T47D cells were cultured in DMEM (LONZA) supplemented with 10% fetal bovine serum (FBS) and with 1% antibiotics (penicillin 100 U ml^{-1} and streptomycin 10 µg ml^{-1}). SUM149 cells were cultured in DMEM/F12 (LONZA) (1:1) supplemented with 10% FBS and with 1% antibiotics. Hs-578-T were cultured in DMEM (Thermo Fisher) supplemented with 10% FBS, glutamine and antibiotics and 10 µg ml^{-1} insulin (Sigma). Mahlavu cells were cultured in EMEM (Sigma) supplemented with 10% FBS, with 1% antibiotics (penicillin 100 U ml^{-1} and streptomycin 10 µg ml^{-1}), 1% MEM NEAA (minimum essential medium non-essential amino acids) and 1% Glutamax. H1299 cells were cultured in RPMI 1640 medium with 10% FBS and 1% antibiotics. MCF7 cells were cultured in EMEM (Sigma) supplemented with 10% FBS, with 1% antibiotics (penicillin 100 U ml^{-1} and streptomycin 10 µg ml^{-1}) and 1% MEM NEAA.

MDA-MB-231 cells, stably expressing GFP–RhoA-G14V and the mutant GFP–RhoA-G14V-F, were maintained in DMEM (LONZA) supplemented with 10% FBS and with 1% antibiotics (penicillin 100 U ml^{-1} and streptomycin 10 µg ml^{-1}) and with addition of selection antibiotics.

MEFs infected with pLPC-RAS^{V12} were maintained as previously described[5].

Mammary epithelial cells were isolated from p53$^{R172H/R172H}$ knock-in mice as previously described[9,41] and seeded on top of 50 kPa or 0.5 kPa Easy Coat hydrogels (Cell Guidance Systems) and harvested after three days. Hydrogels for the experiments in Fig. 5 were as in ref. [33].

Reagents and plasmids. The library of FDA-approved drugs (Screen-Well FDA-Approved Drug Library, 640 chemical compounds dissolved at 10 mM in dimethylsulfoxide) was obtained from Enzo Life Sciences.

The following compounds were purchased from Sigma Aldrich: cerivastatin (SML0005), ouabain (O3125), spiperone (S7395), ivermectin (I888), salmeterol (S5068), simvastatin (S6196), GGTI-298 (G5169), geranylgeranyl pyrophosphate (G6025), zoledronic acid (SML0223), mevalonic acid (41288), cycloheximide (C7698 and C1988), blebbistatin (B0560) and Y-27632 dihydrochloride (Y0503). Latrunculin-A (sc-202691) was purchased from Santa Cruz Biotechnology. The following compounds were purchased from Cayman: YM-53601 (18113), FTI-277 (F9803), Nutlin-3 (10004372) and SAHA (10009929). MG132 (474790) was purchased from Calbiochem. Thioridazine hydrochloride (1306110) was purchased from Tocris. C3-RhoA inhibitor I (CT04) was purchased from Cytoskeleton. Lipoprotein-depleted serum (LDS) (880100-2) was purchased from Biocompare (DBA). Z-Vad FMK was from Enzo Life Science (ALX-260-020-M001). 5-fluorouracile (5FU) was from Teva. Doxorubicin hydrochloride was from Sigma (D1515). Picro Sirus Red Stain Kit (Connective Stain) (ab 150681) was purchased from Abcam.

pEGFP–RhoA-G14V was a gift from C. Schneider (Laboratorio Nazionale CIB, Italy). The retroviral constructs (pLPC) coding for GFP–RhoA-G14V (CLVL) and GFP– RhoA^{V14}-F (CVLS) were generated by PCR mutagenesis from pEGFP–RhoA-G14V[8].

pcDNA3-p53R280K was previously described[5].

High-content screening. For the screening experiments, MDA-MB-231 cells (3.0×10^3 per well) were seeded on black clear-bottom 384-well plates (PerkinElmer). Twenty-four hours later, the FDA-approved drugs were transferred robotically from library stock plates (0.1 mM and 1 mM in DMSO) to the plates containing the cells; controls were added to columns 1, 2, 23 and 24 of each plate. Cells were fixed at 48 h after plating (that is, 24 h after addition of drugs), and processed immediately for immunofluorescence. Briefly, cells were fixed with 4% paraformaldehyde for 15 min, permeabilized with 0.5% Triton X-100 in phosphate-buffered saline (PBS) solution for 10 min, followed by 30 min blocking in 3% FBS. Cells were then incubated with a mouse antibody against mutant p53 (DO-1, Santa Cruz Biotechnology) diluted in blocking solution for 1 h. Cells were further washed with PBS and incubated for 1 h with a secondary antibody conjugated to Alexa Fluor-594 (Life Technologies), and stained with Hoechst 33342 (Life Technologies).

Image acquisition was performed using an ImageXpress Micro automated high-content screening fluorescence microscope (Molecular Devices) at ×10 magnification; a total of 9 images were acquired per wavelength, well and replicate, corresponding to about 4,500 cells analysed per experimental condition and replicate. Image analysis to identify cells presenting mutant p53 signal was performed using the 'Multi-Wavelength Translocation' application module implemented in MetaXpress software (Molecular Devices).

Screening was performed in duplicate, at two drug concentrations (1 µM and 10 µM); the final concentration of DMSO in the culture medium was 1% (v/v) for all experimental conditions. The screening was performed at the ICGEB High-Throughput Screening Facility (http://www.icgeb.org/high-throughput-screening.html).

Transfections. siRNA transfections were performed with Lipofectamine RNAi-MAX (Life Technologies) in antibiotic-free medium according to the manufacturer's instructions. Sequences of siRNAs are reported in Supplementary Table 3. Negative control siRNA was: AllStars negative control siRNA Qiagen 1027281. In Supplementary Fig. 3J, siHDAC6 was transfected two times to improve the efficiency of HDAC6 protein reduction.

DNA transfections were performed in MDA-MB 231 cell lines with Lipofectamine 2000 (Invitrogen) in antibiotic-free medium according to the manufacturer's instructions.

For retrovirus production, low-confluence HEK-293GP packaging cells were transfected with appropriate vectors by calcium phosphate, in combination with pMD2ENV coding for envelope proteins. After 48–72 h the virus-containing medium was filtered and added to target cells. Cells were selected with puromycin (0.5 µg ml^{-1}).

Quantitative real-time PCR. Cells were harvested in Qiazol lysis reagent (Qiagen) for total RNA extraction, and contaminant DNA was removed by DNase treatment. qRT-PCR analyses were carried out on retrotranscribed cDNAs with Quantitect reverse transcription kit (Qiagen) and analysed with Biorad CFX Manager software. Experiments were performed at least three times, with duplicate replicates. The quantification is based on the $2^{-\Delta\Delta Ct}$ method using the housekeeping gene histone 3 (*H3*) as a normalizer. PCR oligonucleotide sequences (F, forward; R, reverse) are reported in Supplementary Table 4. To monitor activation of mutant p53, we measured mRNA expression of the 'ten genes' signature as previously described[5].

Antibodies. The antibodies used for western blot and immunofluorescence were: anti-p53 (1:1,000; DO-1, Santa Cruz Biotechnology), anti-actin (1:5,000; C11, Sigma), anti-GAPDH (1:5,000; MAB374, Millipore), anti-SREBP1 (2A4) (1:500; sc13551, Santa Cruz Biotechnology), anti-SREBP2 (1:500; 557037, BD Bioscience), anti-SCD-1 (1:1,000; ab19862, Abcam), anti-vinculin (1:5,000; V4505, Sigma), anti-Hsp90 (1:1,000; sc13119, Santa Cruz Biotechnology), anti-HDAC6 (H-300) (1:1,000; sc-11420, Santa Cruz Biotechnology), acetylated-lysine antibody (1:1,000; 9441, Cell Signaling), anti-α-tubulin (1:5,000; T5168, Sigma), anti-acetylated-tubulin (1:1,000; T6793, Sigma), anti-GFP (1:1,000; home-made), anti-MDM2 (SMP14; SC-965, Santa Cruz Biotechnology), anti-MLC2 (1:1,000; 3672S, Cell Signaling), anti-pMLC2 (phospho Ser19) (1:1,000; 3675S, Cell Signaling), anti-FAK (C-20) (1:1,000; sc-558, Santa Cruz Biotechnology), anti-pFAK (phospho Tyr397) (1:1,000; ab81298, Abcam), anti-YAP (1:1,000; sc-15407, Santa Cruz Biotechnology), anti-TAZ (1:1,000; HPA007415, Sigma), anti-PSMA2 (1:1,000; sc-54671, Santa Cruz). Phalloidin was from Alexa Fluor (A12379) and anti-BrdU antibody (RPN202) was from GE Healthcare. Anti-cleaved PARP p85 fragment pAb was from Promega (G7341).

Immunofluorescence and western blot. Immunofluorescence staining was performed as previously described[8]. Briefly, cells were fixed in 4% paraformaldehyde for 10 min, washed in PBS, permeabilized with Triton 0.1% for 10 min and blocked in PBS FBS 3% for 30 min. Antigen recognition was performed by incubating primary antibody for 1 h at 37 °C and with goat anti-mouse Alexa Fluor 568 (Life Technologies) as a secondary antibody for 30 min at 37 °C. Nuclei were counterstained with Hoechst 33342 (Life Technologies).

Western blot analysis was performed as previously described[8]. The protein stability determination was performed as previously described[5]. Immunoblots were quantified using the ImageJ program, which measures the integrated density of bands corrected for background. Supplementary Fig 6 shows the average ratio density from at least three experiments ± s.d. Two-tailed Student's *t*-tests were performed to determine the statistical significance.

Co-immunoprecipitation. Co-immunoprecipitation experiments with endogenous proteins were performed using co-immunoprecipitation buffer (NaCl 120 mM, Tris-HCl pH 8 20 mM, EDTA 1 mM, NP40 0.5%) with protease inhibitors. Samples were cleared by centrifugation for 30 min at 13,000*g* at 4 °C and incubated for 2 h at 4 °C with anti-p53 antibody. After 1 h incubation with protein G–Sepharose (GE Healthcare), immunoprecipitates were washed three times in co-immunoprecipitation buffer, resuspended in sample buffer, and analysed by immunoblotting.

For ubiquitylation assays, cells were lysed in 2% SDS, 150 mM NaCl, 10 mM Tris-HCl, pH 8.0, 1 mM phenylmethyl sulfonyl fluoride, 5 mM NaF, 1 mM Na_3VO_4, 0.5% (v/v) sodium deoxycholate with protease inhibitor cocktail (Sigma-Aldrich) and ubiquitin aldehyde 50 ng ml^{-1}. Cell lysates were diluted in immunoprecipitation buffer: 10 mM Tris-HCl, pH 8.0, 150 mM NaCl, 2 mM EDTA and 1% Triton. The anti-p53 antibody (DO-1; Santa Cruz) was covalently bound to protein G Sepharose (Amersham Biosciences, GE Healthcare) using 5 mg ml^{-1} dimethylpimelimidate (Pierce Biosciences, Thermo Fisher Scientific).

Isolation of GTP-loaded RhoA GTPase. The GTP-loaded form of RhoA was pulled down with GST–RHOTEKIN beads (Cytoskeleton), according to the manufacturer's instructions.

Colony-formation assay. Five thousand cells were plated on 6 cm plates. The day after, the medium was supplemented with drugs as indicated in the figures. After 6 days, the cells were fixed with 4% paraformaldehyde (PFA) and stained for 30 min with Giemsa (Fluka) solution diluted 1:5 in water. The plates were washed with water, dried and scanned. Colony quantification was performed using ImageJ.

BrdU incorporation assay. Cells (3×10^4) were plated in 24-well plates. The day after, the medium was supplemented with DMSO or cerivastatin as indicated in the figures. At 48 h following the treatment, the DNA precursor bromodeoxyuridine (BrdU) (20 μM) was added to the medium for 2–12 h before fixation. Briefly, the cells were fixed in 4% paraformaldehyde for 10 min, washed in PBS, permeabilized with Triton 0.1% for 10 min and washed three times with NaOH 50 mM solution and washed in PBS. Primary anti-BrdU antibody solution (1:2 dilution), to detect incorporated bromodeoxyuridine (BrdU), was used for 2 h at 37 °C and goat anti-mouse Alexa Fluor 568 (Life Technologies) was used as the secondary antibody for 1 h a 37 °C. Nuclei were counterstained with Hoechst 33342 (Life Technologies).

Mice and animal care. For in vivo studies, one million MDA-MB-231 cells were resuspended in 100 μl of DMEM, and injected into the mammary fat of previously anaesthetized seven-week-old SCID female mice (1–3% isoflurane, Merial Italia SpA) as previously described[8]. At day 12 after cell injection, the mice were subjected to intravenous injection of zoledronic acid ((1-hydroxy-2-(1*H*-imidazoledronic acid-1-yl) ethylidene) (200 μg kg^{-1} body weight), every 4 days until the end of the experiment (day 40). At day 40, the animals were euthanized and the primary tumours were extracted and directly frozen in liquid nitrogen. Tissues were lysed for immunoblot analysis or sectioned at 5 μm, fixed and stained either with haematoxylin and eosin (H&E) for histological analysis or with Picro Sirius and haematoxylin to perform AFM analysis. Four tumours per group were used. The mice were used and housed in a specific pathogen-free (SPF) animal facility. Procedures involving animals and their care were performed in conformity with institutional guidelines (D.L. 116/92 and subsequent complementing circulars) and all experimental protocols were approved by the ethical Committee of the University of Padua (CEASA). The study is compliant with all relevant ethical regulations regarding animal research.

Microarray analysis for stiffness signature. For microarrays of genes regulated by matrix stiffness uptake, MDA-MB-231 cells were plated on soft fibronectin-coated hydrogels, as compared with the same cells grown on fibronectin-coated rigid surfaces (plastic). For each experimental condition, four biological replicates were prepared and processed in parallel. Total RNA was extracted using TriPure (Roche). RNA quality and purity were assessed on the Agilent Bioanalyzer 2100 (Agilent Technologies); RNA concentration was determined using the NanoDrop ND-1000 Spectrophotometer (NanoDrop Technologies Inc.). Labelling and hybridization were performed according to Affymetrix One Cycle Target Labeling protocol on HG-U133 Plus 2.0 arrays (Affymetrix).

All data analyses were performed in R (version 3.2.4) using Bioconductor libraries (BioC 3.2) and R statistical packages. Probe level signals were converted to expression values using robust multi-array average procedure RMA[42] of Bioconductor affy package. Differentially expressed genes were identified using Significance Analysis of Microarray algorithm coded in the samr R package[43]. In SAM, we estimated the percentage of false-positive predictions (that is, false discovery rate, FDR) with 100 permutations. To identify genes associated with stiffness in cells of mammary origin (stiffness signature), we compared the expression levels of MDA-MB-231 cells grown on stiff (Young's modulus: 50 kPa) and soft hydrogels (Young's modulus: 0.5 kPa) and selected those probe sets with an FDR ≤ 1% and a fold change ≥ 1.5. This selection resulted in 220 probe sets induced in the stiff matrix (Supplementary Table 5).

Atomic force microscopy analysis. AFM was used to investigate cell mechanical properties. In particular, elastic assessment of stiffness was done taking advantage of the force spectroscopy capabilities of a Smena AFM (NT-MDT Co.) mounted on an inverted fluorescence microscope (Nikon Eclipse Ti-U). In brief, force spectroscopy measures the deflection of the AFM cantilever when it is pushed against a surface. Deflection data were subsequently converted into a force versus indentation curve based on cantilever spring constant and displacement knowledge[44]. Compliance of the material under the tip was determined in this work by fitting the data with a Hertzian model of surface indentation[45]. Cell stiffness was established by acquiring a single force spectroscopy curve in the central part of the cell, roughly corresponding to the nucleus position. The AFM tip was placed in the correct position above cells using an inverted microscope in bright field mode. Cells were measured in 1 × PBS buffer at room temperature. For each sample, 60 randomly chosen cells were measured and analysed. Tissue section stiffness was studied by evaluating the stiffness of the cells inside the tissue, marking their nuclei via haematoxylin staining, and ECM stiffness, visualizing it using the collagen- and amyloid-specific dye Picro Sirius Red Stain. AFM force curves were obtained on each sample (4 control, not treated, samples and 4 zoledronate-treated ones) randomly acquiring about 60 curves on blue, haematoxylin-positive, areas and about 60 curves on red, Picro Sirius Red-positive, areas (see Supplementary Fig. S3). A total number of 210 and 245 stiffness values were obtained for controls and treated cells, respectively; 240 and 239 curves were instead acquired for control and treated ECMs. During AFM characterization, sections were maintained immersed in 1 × PBS buffer at room temperature. The cantilever used was a tip-less probe characterized by a spring constant of about 0.03 nN nm^{-1} (HQ:CSC38 cantilevers from MikroMasch Co), at the end of which a 18-μm-diameter silica bead (Thermo Fisher Scientific) was glued using UV curable glue (Norland Products Inc.). Force spectroscopy measurements were performed at constant speed (2.5 μm s^{-1}) and triggered to a maximum force applied to the sample of 5 nN. Elastic modulus values (E), in kPa, were determined by fitting obtained force–displacement curves with a Hertzian model for the tip used taking advantage of the NOVA (NT-MDT Co.) control and analysis software.

Statistics and data processing were performed using Igor Pro software (www.wavemetrics.com) and R statistical computing software (www.R-project.org). The significance of the differences in the data was established as equality of probability distributions via the Kolmogorov–Smirnov test.

Breast cancer gene expression data. We downloaded the METABRIC collection, comprising gene expression data and clinical annotations for 997 breast cancer samples, from the European Genome-Phenome Archive (EGA, http://www.ebi.ac.uk/ega/) under accession number EGAD00010000210 (2012). Original Illumina probe identifiers have been mapped to Entrez gene IDs using the Bioconductor illuminaHumanv3.db annotation package for Illumina HT-12 v3 arrays obtaining $\log_2$ intensity values for a total of 19,761 genes. The TP53 status of 117 samples annotated as 'missense' mutant p53 was derived from ref. [46].

Average signature expression and signature scores. Average signature expression of the mutant-p53 signature[31] and of the YAP/TAZ activity-signature[32] was calculated as the standardized average expression of all signature genes in sample subgroups. Samples were classified as 'stiffness high' or 'stiffness low', summarizing the standardized expression levels of the "stiffness' signature genes into a combined score with zero mean. The values shown in graphs are thus adimensional.

Statistics and reproducibility. The experiment for Fig. 1a was repeated two times. The experiment in Fig. 5d was completed once. All other experiments are representative of at least three independent repeats. Error bars represent mean ± s.d. from $n = 3$ biological replicates. P values were determined using two-tailed Student's t-test as noted in the figure legends.

Life Sciences Reporting Summary. Further information on experimental design is available in the Life Sciences Reporting Summary.

Data availability. Microarray data that support the findings of this study have been deposited in the Gene Expression Omnibus (GEO) under the accession code GSE93529. Gene expression data and clinical annotations for 997 breast cancer samples in the METABRIC collection were downloaded from European Genome-Phenome Archive ((EGA), http://www.ebi.ac.uk/ega/) under accession number EGAD00010000210. Source data for Figs. 1g and 2a, and Supplementary Figs. 1J, 2I, 2K, 3I, 4A–D and 5B are provided in Supplementary Table 6. All other data supporting the findings of this study are available from the corresponding author on reasonable request.

References

41. Rustighi, A. et al. Prolyl-isomerase Pin1 controls normal and cancer stem cells of the breast. *EMBO Mol. Med.* **6**, 99–119 (2014).
42. Irizarry, R. A. et al. Exploration, normalization, and summaries of high density oligonucleotide array probe level data. *Biostatistics* **4**, 249–264 (2003).
43. Tusher, V. G., Tibshirani, R. & Chu, G. Significance analysis of microarrays applied to the ionizing radiation response. *Proc. Natl Acad. Sci. USA* **98**, 5116–5121 (2001).
44. Alonso, J. L. & Goldmann, W. H. Feeling the forces: atomic force microscopy in cell biology. *Life Sci.* **72**, 2553–2560 (2003).
45. Sneddon, I. N. The relation between load and penetration in the axisymmetric Boussinesq problem for a punch of arbitrary profile. *Int. J. Eng. Sci.* **3**, 47–57 (1965).
46. Silwal-Pandit, L. et al. TP53 mutation spectrum in breast cancer is subtype specific and has distinct prognostic relevance. *Clin. Cancer Res.* **20**, 3569–3580 (2014).

Corresponding author(s): Giannino Del Sal

☐ Initial submission ☐ Revised version ☒ Final submission

Reporting Summary

Experimental design

1. Sample size

Describe how sample size was determined.

No statistical method was used to determine sample size. The sample size was chosen to include at least three biological replicates.

2. Data exclusions

Describe any data exclusions.

No data were excluded from the analysis.

3. Replication

Describe whether the experimental findings were reliably reproduced.

Experiments were performed succesfully at least three times. All replication attempts were succesfull.

4. Randomization

Describe how samples/organisms/participants were allocated into experimental groups.

Animals were randomly put into cages and randomly assigned to experimental groups.

5. Blinding

Describe whether the investigators were blinded to group allocation during data collection and/or analysis.

The investigators were not blinded. The experiments were quantified and were relevant appropriate statistical tests performed.

Note: all studies involving animals and/or human research participants must disclose whether blinding and randomization were used.

6. Statistical parameters

For all figures and tables that use statistical methods, confirm that the following items are present in relevant figure legends (or in the Methods section if additional space is needed).

n/a	Confirmed
☐	☒ The exact sample size (*n*) for each experimental group/condition, given as a discrete number and unit of measurement (animals, litters, cultures, etc.)
☐	☒ A description of how samples were collected, noting whether measurements were taken from distinct samples or whether the same sample was measured repeatedly
☐	☒ A statement indicating how many times each experiment was replicated
☐	☒ The statistical test(s) used and whether they are one- or two-sided (note: only common tests should be described solely by name; more complex techniques should be described in the Methods section)
☒	☐ A description of any assumptions or corrections, such as an adjustment for multiple comparisons
☐	☒ The test results (e.g. *P* values) given as exact values whenever possible and with confidence intervals noted
☐	☒ A clear description of statistics including central tendency (e.g. median, mean) and variation (e.g. standard deviation, interquartile range)
☐	☒ Clearly defined error bars

See the web collection on statistics for biologists for further resources and guidance.

Software

Policy information about availability of computer code

7. Software

Describe the software used to analyze the data in this study.	Prism GraphPad was used for all statistical analysis

For manuscripts utilizing custom algorithms or software that are central to the paper but not yet described in the published literature, software must be made available to editors and reviewers upon request. We strongly encourage code deposition in a community repository (e.g. GitHub). *Nature Methods* guidance for providing algorithms and software for publication provides further information on this topic.

Materials and reagents

Policy information about availability of materials

8. Materials availability

Indicate whether there are restrictions on availability of unique materials or if these materials are only available for distribution by a for-profit company.	There are no restrictions for any of the materials

9. Antibodies

Describe the antibodies used and how they were validated for use in the system under study (i.e. assay and species).	Antibodies source was described in method section. The antibodies used for western blot and immunofluorescence were: anti-p53 (1:1000; DO-1, Santa Cruz Biotechnology), anti-Actin (1:5000; C11, Sigma), anti-GAPDH (1:50000; MAB374, Millipore), anti-SREBP1 (2A4) (1:500; sc13551, Santa Cruz Biotechnology), anti-SREBP2 (1:500; 557037, BD Bioscience), anti-SCD-1 (1:1000; ab19862, Abcam), Anti-Vinculin (1:5000; V4505 Sigma), anti-Hsp90 (1:1000; sc13119, Santa Cruz Biotechnology), Acetylated-Lysine Antibody (1:1000; 9441, Cell Signaling), anti-α-Tubulin (1:5000, T5168, Sigma), anti-acetylated-tubulin (1:1000; T6793, Sigma), anti GFP (1:1000; home made), anti-MDM2 (SMP14; SC-965, Santa Cruz Biotechnology), anti-MLC2 (1:1000; 3672S, Cell Signaling), anti-pMLC2 (phospho Ser19) (1:1000; 3675S; Cell signalling), anti-FAK (C-20) (1:1000; sc-558, Santa Cruz Biotechnology), anti-pFAK (phospho Y397) (1:1000; ab81298, Abcam), anti-YAP (1:1000; sc-15407; Santa Cruz Biotechnology),anti-TAZ (1:1000; HPA007415, Sigma), Anti-PSMA2 (1:1000; sc-54571; Santa Cruz). Phalloidin is A12379 (Alexa Fluor), Anti-BrdU antibody (RPN202) is GE Healthcare. Positive and/or negative controls such as protein knockdown, knockout, overexpression were previously used to validate the relevant antibodies used in this work.

10. Eukaryotic cell lines

a. State the source of each eukaryotic cell line used.	ATCC or other laboratories cooperating on the project. Mahlavu cells were a kind gift from Dr. P. Hainaut (Institut Albert Bonniot, La Tronche, France); BT-549 and MDA-MB-468 cells were a kind gift from Dr. G. Blandino (Regina Elena National Cancer Institute, Rome, Italy); SKBR3 were a kind gift from Dr. S. Schoeftner (Department for Life Sciences, University of Trieste, Trieste, Italy)
b. Describe the method of cell line authentication used.	Cells were subjected to STR genotyping with PowerPlex 18D System and confirmed in their identity comparing the results to reference cell databases (DMSZ, ATCC and JCRB databases).
c. Report whether the cell lines were tested for mycoplasma contamination.	Cells were tested for mycoplasma contamination
d. If any of the cell lines used are listed in the database of commonly misidentified cell lines maintained by ICLAC, provide a scientific rationale for their use.	No commonly misidentified cell lines were used

Animals and human research participants

Policy information about studies involving animals; when reporting animal research, follow the ARRIVE guidelines

11. Description of research animals

Provide details on animals and/or animal-derived materials used in the study.	For in vivo studies, one million of MDA-MB-231 cells were resuspended in 100 µL of DMEM, injected into the mammary fat of previously anesthetized 7 weeks old SCID female mice (1–3% isoflurane, Merial Italia S.p.A, Italy) as previously described3. At day 12 after cell injection, mice were subjected to intravenous injection of zoledronic acid ([1-hydroxy-2- (1H-imidazoledronic acid-1-yl) ethylidene] (200 µg/Kg body weight), every 4 days until the end of the experiment (day 40). At day 40 the animals were sacrificed and the primary tumours were extracted and directly frozen in liquid nitrogen. Tissues were lysed for immunoblot analysis or sectioned at 5 µm, fixed, and stained either with hematoxylin and eosin (H&E) for histological analysis or with Picro Sirius and hematoxylin to perform AFM analysis. Four tumors per group were used. The mice were used and housed in a specific pathogen-free (SPF) animal facility. Procedures involving animals and their care were performed in conformity with institutional guidelines (D.L. 116/92 and subsequent complementing circulars) and all experimental protocols were approved by the ethical Committee of the University of Padua (OPBA). the study is compliant with all relevant ethical regulations regarding animal research.

Policy information about studies involving human research participants

12. Description of human research participants

Describe the covariate-relevant population characteristics of the human research participants.	The study does not involve human research participants